PHYSICAL REVIEW C VOLUME 12, NUMBER 5 NOVEMBER 1975

Qualitative behavior of heavy-ion elastic scattering angular distributions*

R. C. Fuller
Brookhaven National Laboratory, Upton, New York 11973
(Received 24 June 1975)

To study the qualitative features of elastic scattering in the presence of strong absorption, the scattering amplitude is decomposed into what the semiclassical approach calls positive- and negative-deflection-angle contributions. For an amplitude obtained from partial-wave summation this is done without approximation by considering the two amplitudes corresponding to the decomposition of each Legendre polynomial into its two traveling-wave components. It is necessary to separately consider the amplitude arising from the infinite-range Coulomb interaction which does not admit a partial-wave expansion. To decompose this amplitude we follow an approach which leads to increased understanding of the "diverging lens" effect of the Coulomb field and the related Fraunhofer and Fresnel diffraction structure of angular distributions. In addition, the absence or presence of oscillation at back angles is shown to be related to the dominance of reflective or "encirclement" scattering. By examining the phase of the positive-deflection-angle contribution to the scattering amplitude, we are able to conclude, in agreement with Frahn, that the smooth fall in tandem heavy-ion elastic angular distributions arises from a diffractive shadow and not a refractive or Coulomb-rainbow shadow.

[NUCLEAR REACTIONS HI elastic angular distributions interpreted.]

I. INTRODUCTION

It has long been realized that Coulomb and strong-absorption effects play an important role in heavy-ion elastic scattering.[1] In the absence of Coulomb interaction, strong absorption gives rise to diffractive angular distributions characterized by marked oscillation in the forward direction. By optical analogy, this is often referred to as Fraunhofer diffraction. In the language of a semiclassical approach this oscillation arises from interference between the positive- and negative-deflection-angle contributions to the scattering amplitude. A more immediately physical interpretation identifies the interfering contributions with waves which have scattered from opposite sides of the interaction region.

With increasing Coulomb interaction Fraunhofer oscillation moves to larger angles. In fact, it is completely absent in much heavy-ion data. Frahn[2] has explained the absence of Fraunhofer diffraction by noting that the repulsive Coulomb interaction provides divergence of the two components which interfere in its absence. In the presence of a sufficiently strong Coulomb force and strong absorption, this implies that one sees only the scattering contribution from one side of the interaction region, and the angular distribution is qualitatively that of Fresnel scattering from a semi-infinite absorptive screen.

Much of the more recent discussion of heavy-ion elastic scattering has stressed the importance of the attractive nuclear interaction and its interplay with the repulsive Coulomb interactions, e.g. Ref. 3. Concentration on these refractive aspects of the scattering problem has led Goldberg and Smith[4] to conclude that the characteristic smooth fall in elastic scattering angular distributions (plotted in ratio to Rutherford) can be interpreted as scattering from the dark side of a "Coulomb rainbow" arising from the dominance of nuclear attraction at small inter-ion separation. This is to be contrasted with Frahn's Fresnel diffraction interpretation in which this smooth fall results from absorption out of the elastic channel. The question is simply which wins—absorption or attraction? In addition, Da Silveira[5] has argued that the oscillation forward of the smooth fall can be understood in terms of the interference on the bright side of a Coulomb rainbow. On the other hand, Rowley and Marty[6] have shown that the smooth-cutoff diffraction model,[7] which contains no rainbow, generates such oscillation by the interference of the dominant Coulomb amplitude with the peripheral component of the nuclear amplitude. Goldberg and Smith[4] stress the importance of a "nuclear rainbow" which can only be studied within an approach which includes nuclear attraction.

The purpose of this paper is the development of consistent concepts appropriate for the qualitative understanding of heavy-ion elastic angular distributions. This requires the study of scattering amplitudes calculated from interactions which include attraction as well as absorption. Phenomenological optical-model potentials are used throughout, although the qualitative conclusions should be valid for folding-model potentials. All arguments will be based on amplitudes obtained by summing the optical-model partial-wave series or,

in many cases, the Rutherford amplitude itself. With this approach we hope to resolve convincingly the conflicting concepts mentioned above which have generally resulted from approximation in the evaluation of the scattering amplitude or approximations to the S-matrix elements.

Our approach will rely on the separate consideration of positive- and negative-deflection-angle contributions to the scattering amplitude.[8] Study of the positive-deflection angle, or "near-side" contribution, leads us to conclude there is generally no "Coulomb rainbow" for the strongly absorptive interactions characteristic of heavy-ion scattering. This result implies that the near-side amplitude probes the entire range of angular momenta or impact parameters in qualitative agreement with Frahn's picture. The far-side amplitude does exhibit behavior which may be interpreted as arising from a nuclear rainbow. Separation of positive- and negative-deflection-angle contributions to the Rutherford amplitude provides quantitative understanding of the "diverging lens" effect of the Coulomb field[2] and shows how the infinite-range Coulomb interaction separates the forward angle far and near scattering contributions, thereby pushing the Fraunhofer diffraction arising from their interference away from forward angles.

It will first be necessary to discuss separation of the far and near elastic amplitudes, which will require an approach which uses a partial-wave expansion of the nuclear amplitude and does not use asymptotic expressions for Legendre polynomials. In turn, this approach is generalized to consider the Rutherford amplitude where a partial-wave expansion is not possible. We then turn to a discussion of angular distributions, which develops a consistent and rather complete qualitative picture of elastic scattering. This discussion relies partially on the study of the phase of the scattering amplitude which leads to the introduction of the concept of local angular momentum.

II. SEPARATION OF "FAR" AND "NEAR" CONTRIBUTIONS TO THE SCATTERING AMPLITUDE

This section will be devoted to the development of work sketched in an earlier paper.[9] Its primary task will be separation of the two components of the scattered wave which emanate from opposite sides of the interaction region. The far and near components of a scattering amplitude obtained from summation over partial waves correspond to replacing the Legendre polynomial by its traveling wave components, $\tilde{Q}_l^{(+)}$ and $\tilde{Q}_l^{(-)}$, respectively[8]; i.e.,

$$P_l(\cos\theta) = \tilde{Q}_l^{(+)} + \tilde{Q}_l^{(-)} \tag{1}$$

where, for large l,

$$\tilde{Q}_l^{(\pm)}(\cos\theta) \sim [2\pi(l+\tfrac{1}{2})\sin\theta]^{-1/2} \exp[\pm i(l+\tfrac{1}{2})\theta - \tfrac{1}{4}i\pi], \quad l^{-1} \lesssim \theta \lesssim \pi - l^{-1}. \tag{2}$$

Friedman, McVoy, and Shuy[10] used these asymptotic expressions for the traveling waves in their study of distorted-wave Born-approximation transfer reaction angular distributions where only peripheral partial waves participate. Since elastic scattering is not entirely peripheral, expressions for the traveling waves valid for all l are required. In terms of the Legendre function of the second kind, $Q_l(\cos\theta)$, they are

$$\tilde{Q}_l^{(\pm)}(\cos\theta) = \tfrac{1}{2}\left[P_l(\cos\theta) \mp i\,\frac{2}{\pi} Q_l(\cos\theta)\right]. \tag{3}$$

Using asymptotic expressions for P_l and Q_l in this equation gives the asymptotic expressions of Eq. (2). The far and near components of an amplitude obtained by partial-wave summation are then given, respectively, by

$$f_F(\theta) = \sum (2l+1) a_l \tilde{Q}_l^{(+)}(\cos\theta) \tag{4a}$$

and

$$f_N(\theta) = \sum (2l+1) a_l \tilde{Q}_l^{(-)}(\cos\theta). \tag{4b}$$

Before decomposing the Coulomb amplitude, where a partial-wave expansion is not possible, it is first useful to study the traveling waves as different continuations of the same function. This will lead to an understanding of how (and when) our physical expectation that near and far amplitudes are continuations of one another through $\theta = 0$ and $\theta = \pi$ is imposed by the traveling waves; i.e., our naive expectation is that positive- and negative-deflection-angle contributions merge at $\theta = 0$ and $\theta = \pi$. We shall find that the fulfillment of this expectation is intimately related to the convergence of the partial-wave expansion.

The single function of interest is the Legendre function of the second kind, $Q_l(z)$, defined in the complex z -plane cut from -1 to $+1$.[11] The average of $Q_l(z)$ across the cut is by definition the Legendre function of the second kind appearing in Eq. (3), i.e.,

$$Q_l(x) = \tfrac{1}{2}[Q_l(x+i\epsilon) + Q_l(x-i\epsilon)]; \quad -1 < x < 1, \quad x = \cos\theta, \tag{5}$$

while its discontinuity across the cut is given by

$$-i\pi P_l(x) = Q_l(x+i\epsilon) - Q_l(x-i\epsilon). \tag{6}$$

The notation in Eq. (5) is confusing but conventional.[12,13] From Eqs. (6), (5), and (3), it follows that the traveling waves are given by the continuation of

$Q_l(z)$ to the cut from above and below, i.e.,

$$\tilde{Q}_l^{(\pm)}(x) = \mp\frac{i}{\pi}Q_l(x \mp i\epsilon)\,. \tag{7}$$

For an amplitude given by a partial-wave series, one may introduce the single amplitude

$$f_Q(z) = \sum (2l+1)a_l Q_l(z) \tag{8}$$

whose continuation gives the far and near amplitudes of Eqs. (4):

$$\begin{aligned} f_F(x) &= -\frac{i}{\pi}f_Q(x - i\epsilon), \\ f_N(x) &= \frac{i}{\pi}f_Q(x + i\epsilon)\,. \end{aligned} \tag{9}$$

Since $Q_l(z)$ may be analytically continued around its branch points at $z=1$ and $z=-1$, so may $f_Q(z)$, and therefore Eq. (9) shows that $f_{F(N)}(x)$ is the continuation of $-f_{N(F)}(x)$ when the branch points are encircled, i.e., the magnitudes of the far and near amplitudes merge at $\theta=0$ and $\theta=\pi$ if the partial-wave series for the full amplitude converges.

These arguments assume that the singularities in the far and near amplitude allow their continuation into a region of the z plane near the cut. In writing a partial-wave series for the amplitude, we have implicitly assumed that the singularities of the scattering amplitude $f(z)$, continued into the complex z plane, lie some distance from the cut; i.e., any finite sum of partial waves is a polynomial in x which cannot represent a function with singularities close to the cut. More rigorously, the partial-wave series of $f(z)$ converges within an ellipse whose foci lie at $z=1$ and $z=-1$, which passes through the singularity of $f(z)$ nearest the cut.[14] In any case, the partial-wave series for the so-called nuclear amplitude encountered in charged-ion scattering presents no problems and its far and near amplitudes merge at $\theta=0$ and $\theta=\pi$ in the manner discussed above. This will be seen explicitly in calculations discussed in a later section.

Not surprisingly, this is not the case for the Coulomb amplitude. Simple classical considerations would argue that repulsive Coulomb scattering has only a positive-deflection-angle contribution and, in fact, this is almost the case. The long-range character of the Coulomb force leads to the contribution of all partial waves in the forward direction; the Coulomb amplitude is singular at $\theta=0$, where the partial-wave series diverges. The singularity at $\theta=0$ is a branch point, since the Rutherford amplitude is given by

$$\begin{aligned} f_R(\theta) &= -\frac{\eta}{2k^2\sin^2\frac{1}{2}\theta}\exp[2i\sigma_0 - i\eta\ln\sin^2(\tfrac{1}{2}\theta)] \\ &= f_R(\pi)\left(\frac{1-x}{2}\right)^{-1-i\eta}. \end{aligned} \tag{10}$$

The cut emanating from this singularity will render continuation of the far and near amplitudes into one another at $\theta=0$ impossible, and this leads to the dominance of the positive-deflection-angle contribution in the forward direction. On the other hand the Coulomb amplitude is regular near back angles where the positive-deflection-angle amplitude continues to a nonzero negative deflection-angle amplitude. This "leakage" around $\theta=\pi$ is responsible for the existence of a negative-deflection-angle contribution.

To decompose the Coulomb amplitude we need an approach which projects the traveling-wave components from the full amplitude since the Coulomb amplitude does not admit a partial-wave expansion. It is first useful to see how the partial traveling wave is obtained from the Legendre polynomial. The analytic properties of $Q_l(z)$ reflected in Eqs. (5) and (6) lead to the equation

$$Q_l(z) = \frac{1}{2}\int_{-1}^{1} dt(z-t)^{-1}P_l(t) \tag{11}$$

for z not on the cut. If we introduce the amplitude $f_Q(z)$ by

$$f_Q(z) = \frac{1}{2}\int_{-1}^{1} dt(z-t)^{-1}f(t)\,, \tag{12}$$

then the far and near amplitudes for an amplitude which admits a partial-wave expansion follow upon interchanging the order of summation over partial waves and integration in Eq. (12) and using Eqs. (11), (8), and (9). Obviously, Eq. (12) may be used to obtain the amplitude $f_Q(z)$ directly from the full amplitude, and the continuation of $f_Q(z)$ prescribed by Eqs. (9) then gives the desired decomposition. We follow this approach for the Coulomb amplitude and check the result by direct calculation. Underlying this approach is the assumption that Eq. (12) provides the appropriate continuation of the amplitude into the complex z plane to allow use of Eqs. (9).

Substitution of the Rutherford amplitude Eq. (10) into Eq. (12) gives

$$f_{R,Q}(z) = \tfrac{1}{2}f_R(\pi)\frac{2}{z+1}\int_0^1 dv\left(1-\frac{2}{z+1}v\right)^{-1}(1-v)^{-1-i\eta}. \tag{13a}$$

The integral is a hypergeometric function.[12] Rather straightforward manipulation yields

$$f_{R,Q}(z) = \tfrac{1}{2}f_R(\pi)\left\{-(1+i\eta)^{-1}F(1,1+i\eta,2+i\eta,\tfrac{1}{2}(1-z)) + \frac{i\pi}{\sinh\pi\eta}(z-1)^{-1-i\eta}\right\}, \tag{13b}$$

where the hypergeometric function $F(1, 1+i\eta, 2+i\eta, \frac{1}{2}(1-z))$ is continuous across the cut, while the second term has a branch point at $z=1$. We take the cut emanating from this branch point to be along the real axis, $\mathrm{Re}(z)<1$. Continuation to the cut as prescribed by Eqs. (9) follows upon taking $x \pm i\epsilon - 1 = (1-x)e^{\pm i\pi}$ which gives

$$f_{R,N}(\theta)/f_R(\theta) = (1-e^{-2\pi\eta})^{-1} - \frac{i}{2\pi}[\sin^2(\tfrac{1}{2}\theta)]^{1+i\eta} S(\theta), \tag{14a}$$

$$f_{R,F}(\theta)/f_R(\theta) = -e^{-2\pi\eta}(1-e^{-2\pi\eta})^{-1} + \frac{i}{2\pi}[\sin^2(\tfrac{1}{2}\theta)]^{1+i\eta} S(\theta), \tag{14b}$$

where

$$S(\theta) = (1+i\eta)^{-1} F(1, 1+i\eta, 2+i\eta; \sin^2(\tfrac{1}{2}\theta)) = \sum_{k\geq 0} \frac{(1+i\eta)_k}{k!}[\psi(k+1) - \psi(k+1+i\eta) - \ln\cos^2(\tfrac{1}{2}\theta)]\cos^{2k}(\tfrac{1}{2}\theta). \tag{15}$$

Again, notation in Eq. (15) follows Ref. 12. We will find the near-Rutherford amplitude dominant at forward angles while the near and far amplitudes merge at back angles. This implies that the first term in Eq. (14a) is dominant at forward angles for a repulsive Coulomb interaction. Note that the algebraic values of the first terms of Eqs. (14a) and (14b) are interchanged for Coulomb attraction, leading to the expected far-side dominance at forward angles for attraction.

Before discussing optical-model calculations it is useful to display some simple properties of the traveling-wave Legendre functions. The Legendre function of the second kind, $Q_l(z)$, which we have previously introduced, is given by[12]

$$Q_l(z) = \tfrac{1}{2}P_l(z)\ln\left(\frac{z+1}{z-1}\right) - W_{n-1}(z), \tag{16}$$

where $W_{n-1}(z)$ is a polynomial in z of degree $n-1$. Continuation to the cut from above and below is again effected by replacing $z-1$ by $(1-x)e^{\pm i\pi}$ to give

$$Q_n(x \pm i\epsilon) = \tfrac{1}{2}P_n(x)\left[\mp i\pi + \log\left(\frac{1+x}{1-x}\right)\right] - W_{n-1}(x). \tag{17}$$

The logarithmic singularities at $x=1$ and -1 are "soft" and generally present no problems. Figure 1 shows plots of $(\sin\theta)^{1/2}|\tilde{Q}_l(\cos\theta)|$ for lower partial waves. Indicated in each of the plots is the asymptotic value $[2\pi(l+\frac{1}{2})]^{-1/2}$ of this quantity as given by Eq. (2).

The orbital angular momentum is just the angular frequency of the asymptotic traveling partial waves, i.e., for

$$\tilde{Q}_l^{(\pm)}(\cos\theta) = |\tilde{Q}_l{}^{\pm}(\cos\theta)|\, e^{\pm\phi_l(\theta)}, \tag{18}$$

$$\frac{d\phi_l}{d\theta} \sim (l+\tfrac{1}{2}). \tag{19}$$

Figure 2 shows plots of the phase derivative of $\tilde{Q}_l^{(+)}$ for the same l's used in the previous plots. Again the asymptotic values are indicated. All phase derivatives in this paper are numerically evaluated by the two-point formula

$$\frac{d\phi}{d\theta} \approx \frac{\phi(\theta) - \phi(\theta-\Delta)}{\Delta} \tag{20}$$

with $\Delta = \frac{1}{2}^\circ$. These plots, along with Fig. 1, indicate that the asymptotic expression is valid in at least the angular region indicated in Eq. (2).

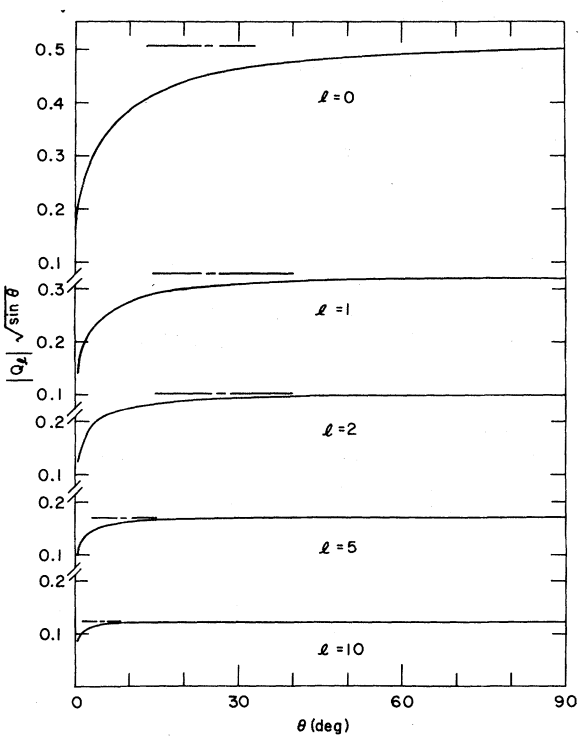

FIG. 1. The magnitude of the traveling-wave Legendre function plotted as $|\tilde{Q}_l(\theta)|\, x\, (\sin\theta)^{1/2}$ for the l values indicated. The asymptotic value $[2\pi(l+\frac{1}{2})]^{1/2}$ is indicated by the dash-dot lines.

III. ILLUSTRATIVE CALCULATIONS AND DISCUSSION

A. Near-far decomposition and interference

All calculations in this paper utilize Woods-Saxon form factors in both the real and imaginary parts of the optical potential. The parameters used in the calculations are given in Table I. These particular potentials were used simply because their angular distributions illustrate a wide range of interference patterns. Their angular distributions will be interpreted in the full angular range, although they were generally fitted to data only in the forward hemisphere. S-matrix elements are generally calculated by the optical-mode code ABACUS.[15] In the customary fashion the Rutherford amplitude, Eq. (10), is isolated in the calculation of the elastic scattering amplitude to give

$$f(\theta)=f_R(\theta)+\tilde{f}(\theta), \tag{21}$$

where $\tilde{f}(\theta)$ is obtained from a partial-wave expansion in terms of the point-Coulomb phase shift σ_l and the so-called nuclear S matrix $\tilde{S}_l$ as

$$\tilde{f}(\theta)=(2ik)^{-1}\sum_{l\geq 0}(2l+1)e^{2i\sigma_l}(\tilde{S}_l-1)P_l(\cos\theta). \tag{22}$$

Equations (14a), (14b), (4a), and (4b) give the far and near amplitudes

$$f_{N(F)}(\theta)=f_{R,N(F)}(\theta)+\tilde{f}_{N(F)}(\theta), \tag{23}$$

where

$$\tilde{f}_{N(F)}(\theta)=(2ik)^{-1}\sum(2l+1)e^{2i\sigma_l}(\tilde{S}_l-1)\times\tilde{Q}_l^{(\mp)}(\cos\theta). \tag{24}$$

We refer to $|f_{N(F)}(\theta)|^2$ as the "near (far) differential cross section" or the "near (far) angular distribution". We shall often plot the differential cross section $d\sigma/d\theta=2\pi\sin\theta(d\sigma/d\Omega)$ since this quantity can be more amenable to theoretical interpretation. In addition, we shall have occasion to study the "nuclear amplitude" $\tilde{f}(\theta)$ separately and shall refer to $|\tilde{f}_{N,(F)}(\theta)|^2$ as the near (far) nuclear differential cross section or the near (far) nuclear angular distribution.

The first set of calculations illustrates both the dominance of positive-deflection-angle Coulomb scattering at forward angles and the importance of the negative-deflection-angle Rutherford amplitude at large angles. In addition, the difference in the back-angle angular distributions of far- and near-

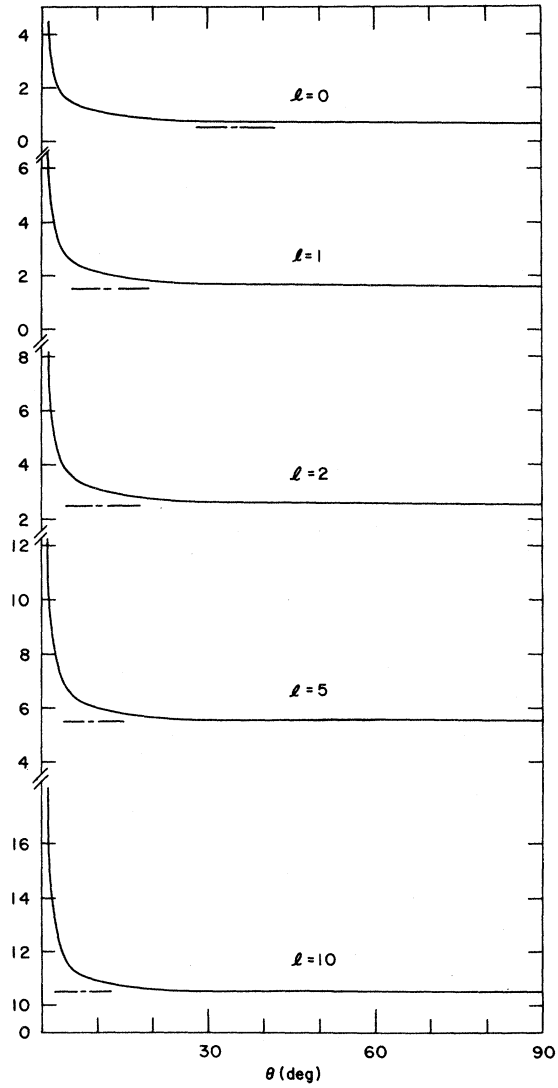

FIG. 2. The derivative with respect to the angle θ of the phase of the traveling wave $\tilde{Q}_l(\theta)$. Its asymptotic value, $l+\frac{1}{2}$, is indicated by the dash-dot line.

TABLE I. Optical model parameters. The radii are $r_0(A^{1/3}+A^{2/2})$.

	Real			Imaginary		
	Strength (MeV)	Radius r_0 (fm)	Diffuseness (fm)	Strength (MeV)	Radius r_0 (fm)	Diffuseness (fm)
56 MeV ^{16}O on ^{16}O	− 17	1.35	0.49	−34.9	0.83	0.805
56 MeV ^{16}O on ^{48}Ca	− 37	1.35	0.42	−78	1.27	0.28
96 MeV ^{12}C on ^{208}Pb	− 40	1.256	0.560	−25	1.256	0.560
46 MeV ^{12}C on ^{26}Mg	−100	1.24	0.48	−27	1.36	0.22

side dominated angular distributions is discussed. Figures 3, 4, and 5 show calculations for 56 MeV ^{16}O scattering from ^{48}Ca. The optical potential is taken from Ref. 16. Figures 3 and 4 show the far and near angular distributions calculated with the naive assumption that the Rutherford amplitude is totally near-sided along with those calculated with the correct decomposition; i.e., the naive approach adds the full Rutherford amplitude, Eq. (10), to the near-nuclear amplitude and takes for the far amplitude only the far-nuclear amplitude of Eq. (24), while the correct approach uses Eq. (14) in Eq. (23). The near-sided nature of the Coulomb amplitude at forward angles is indicated by the agreement of the two calculations for both the near and far angular distributions in the forward direction. The importance of the correct near- and far-side Rutherford amplitudes is indicated by the divergence of the naive from the correct calculations at larger angles.

The full and far-side differential cross sections are plotted in Fig. 5. First note the dominance of the near amplitude which is also apparent in comparing Figs. 3 and 4. This follows from the dominance of Coulomb scattering at forward angles and, as discussed previously, the singularity in the Rutherford amplitude which leads to a "jump" discontinuity in going from the far to the near Rutherford amplitudes at the $\theta = 0$. It is this discontinuity which provides the "divergent lens" effect[2] of the repulsive Coulomb field by guaranteeing that the near-side amplitude predominates at forward angles, thereby pushing oscillation arising from its interference with the far-side amplitude to larger angles. By comparing the near-side angular distribution of Fig. 3 with the full angular distribution in Fig. 5, we conclude that the very weak oscillation in the full angular distribution for $80° \lesssim \theta \lesssim 140°$ arises from interference with the far-side amplitude.

Two features of the angular distributions in Fig. 5 still require explanation; first, the oscillation in the far-side amplitude at large angles and second, the absence of oscillation at back angles in the full amplitude even though the magnitudes of the far and near amplitudes differ by less here than in the mid-angular range where their interference, although weak, is apparent. These two features have a common explanation which follows from the merging of the far and near amplitudes at $\theta = \pi$. As will be shown later, the near-side amplitude at large angles is the reflection amplitude for small impact parameter or, equivalently, small angular momentum trajectories. If the far-side amplitude is to merge with the near-side amplitude it can

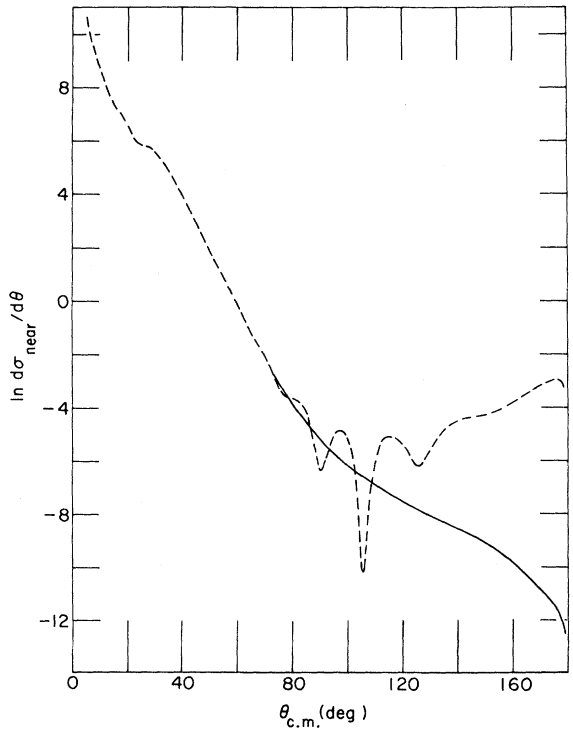

FIG. 3. Logarithmic plots of $\sin\theta|f_{near}|^2 = d\sigma_{near}/d\theta$ for 56 MeV ^{16}O on ^{48}Ca. The dashed line shows the naive calculation which assumes Rutherford scattering in near-sided, while the solid line uses Eq. (14a) for the near-Rutherford amplitude.

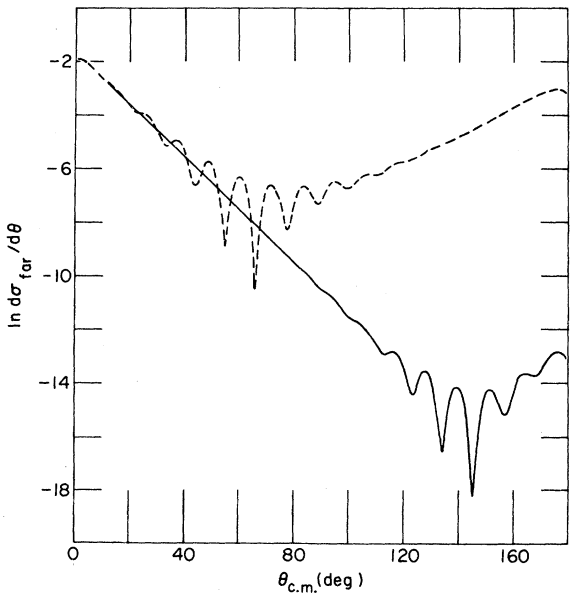

FIG. 4. Plots of far-side quantities for 56 MeV ^{16}O on ^{48}Ca. The dashed line shows the naive calculation which assumes there is no far-side contribution to the Rutherford amplitude and the solid line uses Eq. (14b) for the far-Rutherford amplitude.

only contain small angular momentum components near $\theta = \pi$. Again, it will be shown that the rate of change of the phase of an amplitude is a measure of its angular momentum content, small angular momentum implying a slowly varying phase. If both the near and far amplitudes have slowly varying phases, the interference cannot range from constructive to destructive and there will be no oscillation in the angular distribution.

In this case we know the nature of the far amplitude forward of its oscillation. The linear fall in the far angular distribution $d\sigma_{\text{far}}/d\theta$ is the signature of the Regge pole previously discussed for this potential (8) and found by Wolter's code.[17] The angular dependence of the amplitude for the pole at the complex angular momentum $\alpha = \alpha_1 + i\alpha_2 = 31.7 + 2.8i$ is just $e^{i(\alpha+1/2)\theta}$. If this pole contribution interferes with an amplitude $n(\theta)$ whose phase is slowly varying, the angular distribution is approximately

$$|n(\theta) + \xi e^{i(\alpha+1/2)\theta}|^2 \approx n(\theta) + |\xi|^2 e^{-2\alpha_2\theta} + 2n(\theta)|\xi| \cos[(\alpha_1 + \tfrac{1}{2})\theta - \chi] , \tag{25}$$

since $n(\theta)$ may be taken to be real without loss of generality. This would predict a valley to valley spacing of $\Delta\theta = 2\pi/(\alpha_1 + \frac{1}{2}) \approx 11°$, which agrees with the period of oscillations in the far-angular distribution and leads to the conclusion that the far-side amplitude backward of the regular oscillation indeed has a slowly varying phase. Physically, near-side dominance implies that the back-angle scattering arises from small impact-parameter reflection whose signature is the absence of back angle oscillation in the full angular distribution.

Figure 6 shows the far-side, near-side, and total unsymmetrized angular distributions for ^{16}O-^{16}O elastic scattering at 26 MeV center-of-mass energy for the extensively studied[17-19] potential introduced by Maher *et al.*[20] Here the Coulomb deflection is weaker and the far-side amplitude is less strongly damped than for ^{16}O-^{48}Ca scattering. Still the predominantly near-sided Rutherford amplitude enforces near-side domination at forward angles and the Fraunhofer diffraction oscillation resulting from the interference of the far and near amplitudes is pushed away from the forward direction to $\theta \approx 60°$. This Fraunhofer diffraction oscillation must appear in angular distributions dominated by far-side scattering at large angles simply because the near-side amplitude is dominant at forward angles. In contrast to the ^{16}O-^{48}Ca case, where the back-angle scattering is dominantly near-sided, we now have back-angle oscillation. This obviously arises from interference of the dominant far-side amplitude with its continuation to the near-side amplitude at $\theta = \pi$. Again the

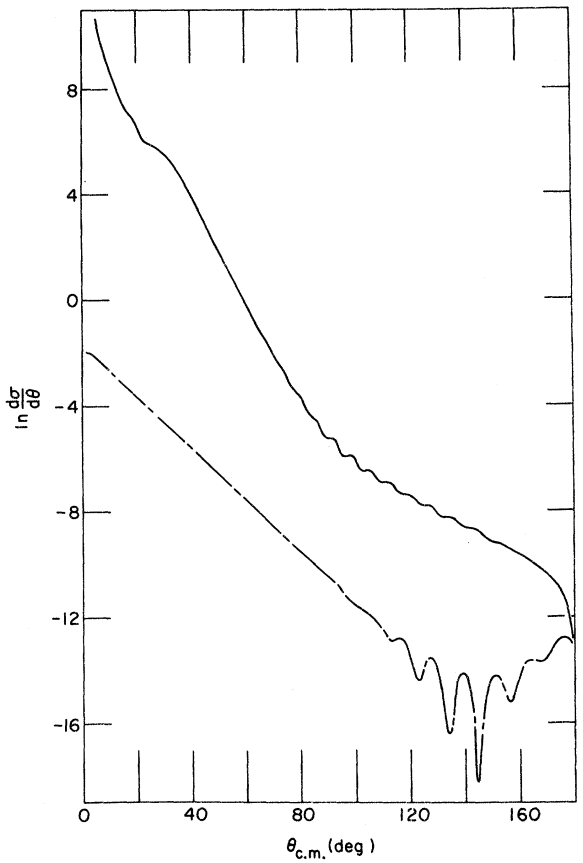

FIG. 5. The solid line is the logarithmic plot of $d\sigma/d\theta$ for 56 MeV ^{16}O on ^{48}Ca. The dash-dot line repeats the correct far-side calculation shown in Fig. 4.

linear fall in the far-side angular distribution is the signature of a Regge pole which Tamura and Wolter[17] have found at $\alpha = 19 + 1.4i$. This pole results in a far-side amplitude

$$e^{-i(\alpha+1/2)(\pi-\theta)} = e^{-i(\alpha+1/2)\pi} e^{-\alpha_2\theta} e^{+i(\alpha_1+1/2)\theta}$$

and a near-side amplitude

$$e^{+i(\alpha+1/2)(\pi-\theta)}$$

near $\theta = \pi$; i.e., for $\theta \approx \pi$, the angular dependence of the scattering amplitude is given by $P_\alpha(-\cos\theta)$, resulting in back-angle oscillation given by $\cos[2(\alpha_1 + \frac{1}{2})\theta]$. Again we have interference structure in the dominated component, which is now the near-side contribution. This can be interpreted as the interference of the Regge pole component, which ties onto the dominant far-side amplitude at $\theta = \pi$, with the essentially reflective component at smaller angles. Again, the angular distance between the two valleys is roughly what this picture would lead us to expect.

We have chosen amplitudes whose far-side components are Regge-pole dominated because we

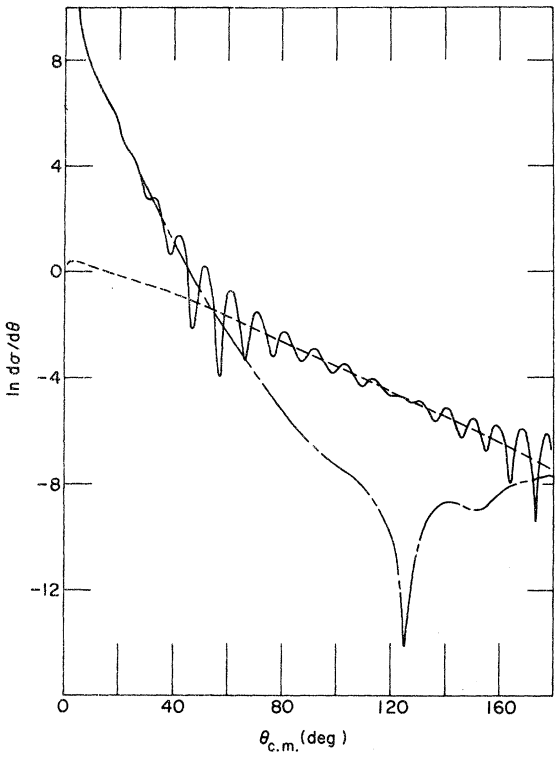

FIG. 6. Logarithmic plots of $d\sigma/d\theta$ (solid), $d\sigma_{near}/d\theta$ (dash-dot), and $d\sigma_{far}/d\theta$ (dash) for 28 MeV (c.m.) ^{16}O-^{16}O elastic scattering.

could then cleanly interpret interference structure in the angular distributions. However, we will find that the far-side amplitude generally describes peripheral components of wave function which have encircled the interaction region, while the near-side amplitude at large angles describes small-impact-parameter reflection. The arguments concerning the "splice" in the dominated amplitude and the existence of back-angle oscillation depend only on these attributes of the far and near amplitudes. Supporting evidence for this assertion is the smooth back-angle angular distribution of the far-side dominated cross section of Fig. 8 and the oscillation at back angles in the far-side dominated α-^{58}Ni angular distribution shown in Ref. 9.

In this connection it is interesting to recall Austern's[21] "black nucleus" model of strong absorption which follows from the imposition of an incoming boundary condition on the three-dimensional wave equation at the "nose" of the interaction region; the wave function is constrained to be totally incoming for $\theta = \pi$ at the interaction radius. Austern found the angular distribution oscillated at back angles and this was shown in Ref. 22 to arise from the encirclement component of the scattering wave function.

Although heavy-ion elastic scattering is known to be absorptive, the quantitative nature of that absorption is an open and difficult experimental question. It should be recalled, however, that "encirclement-component" domination of back angles requires the far-side amplitude to pass through the near-side amplitude, which necessarily predominates at forward angles. The resulting interference oscillation in the angular distribution will appear at forward angles where cross sections are generally larger than at extreme back angles.

B. Angular dependence of near-side scattering

We now address the problem of contradictory explanations of the qualitative features of heavy-ion angular distributions. In the language used in this paper our concern is the near-side amplitude which is generally the dominant amplitude in tandem heavy-ion experiments. When plotted in ratio to the Rutherford cross section the angular distribution consists of oscillation, decreasing in frequency and increasing in magnitude, followed by a precipitous and smooth fall. As mentioned earlier, this has been interpreted as the signature of a Coulomb rainbow[4,5] or of Fresnel diffraction.[2] The resolution of this contradiction is important because the two interpretations can imply that quite different

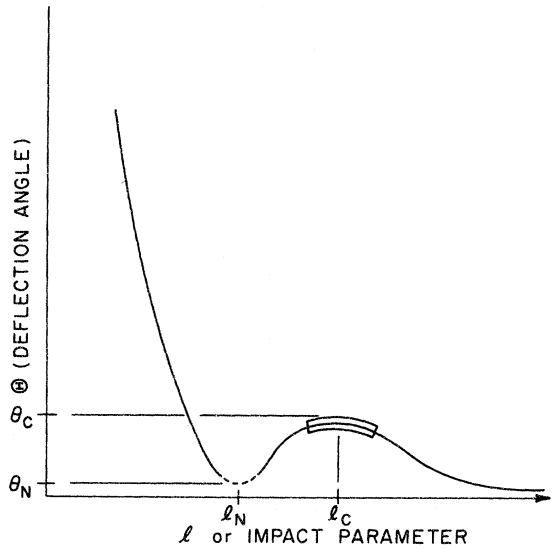

FIG. 7. Schematic plot of the deflection angle typical of heavy-ion calculations. The portion of the curve around the local maximum is enclosed to indicate that the dark-side, $\Theta > \Theta_c$, of the Coulomb rainbow arises from a localized set of angular momenta. For the dashed region around the local minimum the same comment applies to the dark side, $\Theta < \Theta_N$, of the nuclear rainbow.

portions of the interaction region are being probed. We shall discuss rainbows and then ask if we are seeing a Coulomb rainbow. Since the answer is no, we then discuss the problem in terms of absorption or diffraction.

The dark side of a rainbow is associated with a classically inaccessible scattering region. Classical positive-deflection-angle scattering is limited to forward angles because the attractive nuclear interaction bends small impact-parameter trajectories forward. However, the effective attractive force is generally, at most, sufficient to bend trajectories to a limited negative deflection angle which restricts classical negative-deflection-angle scattering to forward angles. Figure 7 is a schematic plot of a deflection function which is typical of heavy-ion scattering and which suggests the Coulomb- and nuclear-rainbow interpretation. The Coulomb rainbow is associated with the local maximum, while the local minimum is associated with the nuclear rainbow. Expansion of the deflection function $\Theta(l)$ about a local extremum at $l = l_R$ yields for the positive- and negative-deflection-angle rainbows the respective amplitudes

$$f_R^{(\pm)}(\theta) = e^{\mp i\phi_R(\theta)} A_\pm(\theta), \tag{26}$$

where

$$\phi_R(\theta) = (l_R + \tfrac{1}{2})\theta + \xi, \tag{27}$$

with ξ constant, contains the rapidly varying component of the phase.[23] On the dark side of a rainbow, $|\theta| > |\theta_R|$, $|A_\pm(\theta)|$ falls rapidly and smoothly, describing propagation into a classically forbidden angular region, while on the bright side $|\theta| < |\theta_R|$, interference from different branches may give rise to oscillation in $|A(\theta)|$. In any case, the signature of a rainbow resides both in the magnitude and the phase of the amplitude. Frahn[2] has shown how strong absorption can give rise to a diffractive shadow described by an amplitude whose magnitude falls smoothly but which has a different phase dependence than the amplitude describing the refractive shadow on the dark side of a rainbow. This difference in phase dependence allows us to distinguish between the two interpretations.

The derivative of the phase of the scattering amplitude is obtained numerically by using Eq. (20). The signature of a Coulomb rainbow is then an approximately constant phase derivative for the near-side amplitude, as is indicated by Eq. (27). Calculations displayed in this discussion use one of two optical-model potentials; (a) a potential fit by a Saclay collaboration[24] to 46 MeV ^{12}C elastic scattering from ^{26}Mg, and (b) a potential fit by an Oak Ridge collaboration[25] to 96 MeV ^{12}C scattering from ^{208}Pb. Both potentials are given in Table I.

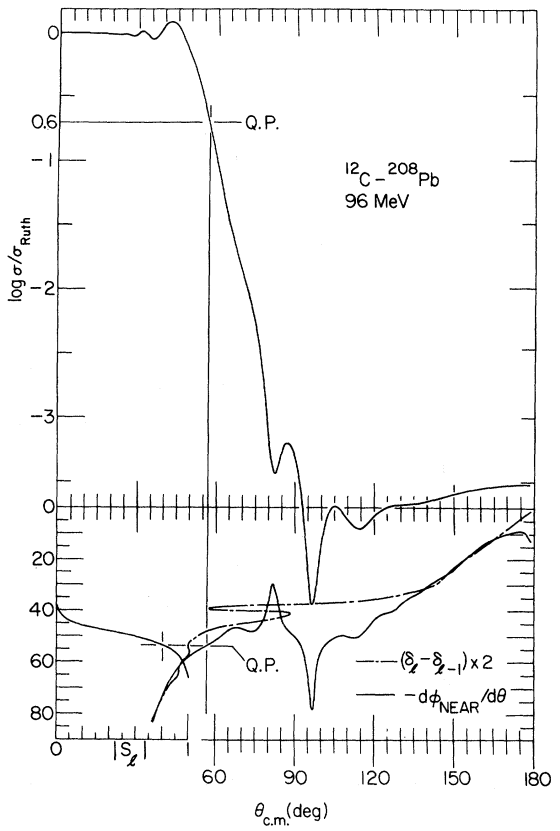

FIG. 8. 96 MeV ^{12}C-^{208}Pb calculations. Upper plot shows $\sigma(\theta)/\sigma_{\text{Ruth}}(\theta)$. The lower portion of the figure shows superposed plots of three quantities. The ordinate indicates l both for the reflection coefficient $|S_l|$ plotted on the left, and for the deflection function (dash-dot) $2(\delta_l - \delta_{l-1})$, where δ_l is the sum of the nuclear and Coulomb phase shifts. The ordinate also indicates values of the phase derivative $d\phi_{\text{near}}/d\theta$ of the near-side scattering amplitude. The quarter-point (Q.P.) value of $\sigma(\theta)/\sigma_{\text{Ruth}}(\theta)$ corresponds to the value of the phase derivative indicated. In turn, this value of the phase derivative is associated with the angular momentum to give a qualitative indication of the l values scattered to the quarter point of $\sigma(\theta)/\sigma_{\text{Ruth}}(\theta)$.

The upper plot of Fig. 8 shows $\sigma/\sigma_{\text{Ruth}}$ for the completely near-side dominated ^{12}C-^{208}Pb calculation. The lower portion of the figure shows the phase derivative of the near-side amplitude. The same plot also shows the deflection function obtained numerically from the Coulomb-plus-nuclear phase shifts. The abscissa for this plot gives the deflection function while the ordinate gives the l value. The reflection coefficient is also plotted. Note that there is no angular region where the phase derivative is approximated by a constant, although the deflection function has a local maximum at $l \sim 57$.

The upper plot of Fig. 9 shows $\sigma/\sigma_{\text{Ruth}}$ for the

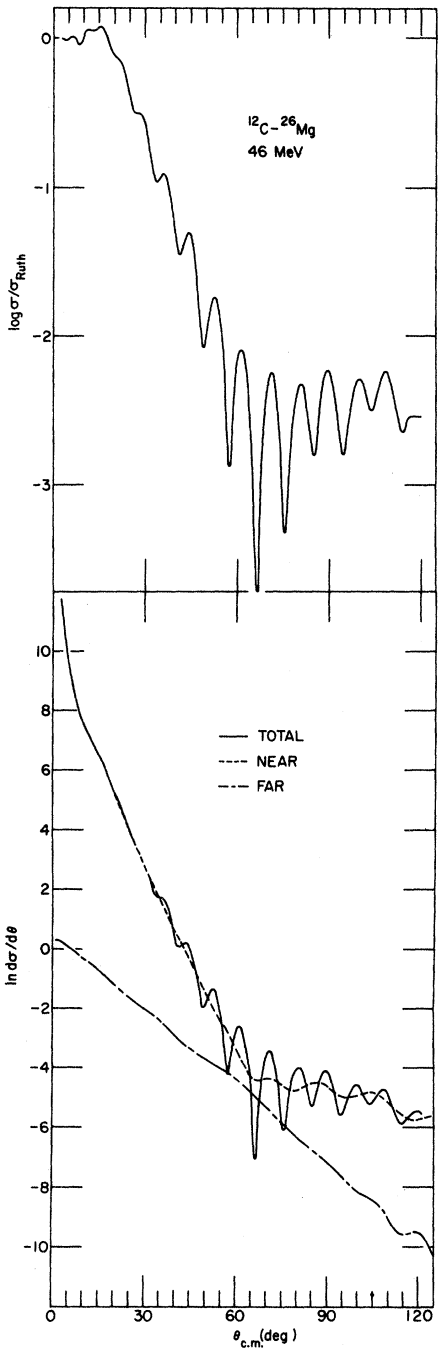

FIG. 9. The upper plot shows $\sigma(\theta)/\sigma_{\mathrm{Ruth}}(\theta)$ for 46 MeV ^{12}C scattering from ^{26}Mg. The lower plot shows $d\sigma/d\theta$ (solid) as well as the far-side angular distribution $d\sigma_{\mathrm{far}}/d\theta$ (dash-dot), and the near-side angular distribution $d\sigma_{\mathrm{near}}/d\theta$ (dash). Interference of the single-side contributions is apparent in the full angular distribution.

^{12}C-^{26}Mg calculation while the lower plot shows how the oscillation in the angular distribution arises from far-near interference even though the near amplitude is dominant over the entire angular range. For this potential Fig. 10 contains the same information as the lower plot of Fig. 8 with the addition of a plot of the phase derivative of the far-side amplitude. Again, the near-side phase derivative is not anywhere constant as it would be for a Coulomb rainbow, although the local maximum in the deflection function is here more pronounced than in the previous case. The far-side amplitude does exhibit the phase behavior of a nuclear rainbow. In fact, the linear fall in the far-side angular distribution, $d\sigma_{\mathrm{Far}}/d\theta$, in Fig. 9 implies that this is an example of what McVoy has called a Regge rainbow.[26]

Having failed to find Coulomb-rainbow behavior in the near-side amplitude, we turn to a diffraction explanation of the *qualitative* behavior of the near-side angular distribution. In the following discussion it is assumed that the angular distribution is near-side dominated and therefore the full amplitude is well approximated by the near amplitude.

The first problem to be confronted is the formation of a shadow by absorption. The shadow in question occurs at larger angles which, in the classical picture, correspond to absorbed trajectories. This implies that the reflection coefficients for angular momenta associated with these trajectories are small, i.e., $|S_l| \ll 1$ for $l < l_p$ where l_p is the angular momentum of a peripheral trajectory. The nuclear amplitude [Eq. (22)] for the scattering of these absorbed partial waves is then

$$f_{\mathrm{abs}}(\theta) \approx (2ik)^{-1} \sum_{l \geq 0}^{L} (2l+1) e^{2i\sigma_l} (-1) P_l(\cos\theta), \qquad L \lesssim l_p . \quad (28)$$

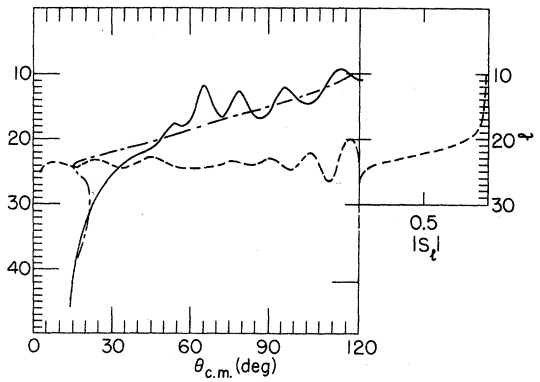

FIG. 10. The same quantities appearing in the lower portion of Fig. 8 are here plotted for 46 MeV ^{12}C on ^{26}Mg with the addition of the phase derivative $+d\phi_{\mathrm{far}}/d\theta$ (dash) of the far-side phase derivative. $-d\phi_{\mathrm{near}}/d\theta$ (solid), and the deflection function $-2(\delta_l - \delta_{l-1})$ (dash-dot) are shown with the conventions of Fig. 8 for the ordinate. The reflection coefficient is shown on the left.

On the other hand, the phase of the Rutherford amplitude, $\phi_{\mathrm{Ruth}}(\theta) = -\eta \ln \sin^2\theta/2\eta$, has the phase derivative

$$d\phi_{\mathrm{Ruth}}/d\theta = -\eta \cot\tfrac{1}{2}\theta\,, \tag{29}$$

which if identified with the angular momentum l yields the classical Coulomb relation

$$\theta = 2\tan^{-1}(\eta/l)\,. \tag{30}$$

Since the Coulomb phase shifts satisfy the recursion relation

$$2(\sigma_l - \sigma_{l-1}) = 2\tan^{-1}(\eta/l)\,, \tag{31}$$

where the left-hand side is approximately the Coulomb deflection function $2d\sigma_l/dl$, Eq. (30) also follows from the stationary phase evaluation of the semiclassical partial-wave integral involving the Coulomb S-matrix alone. For angles satisfying

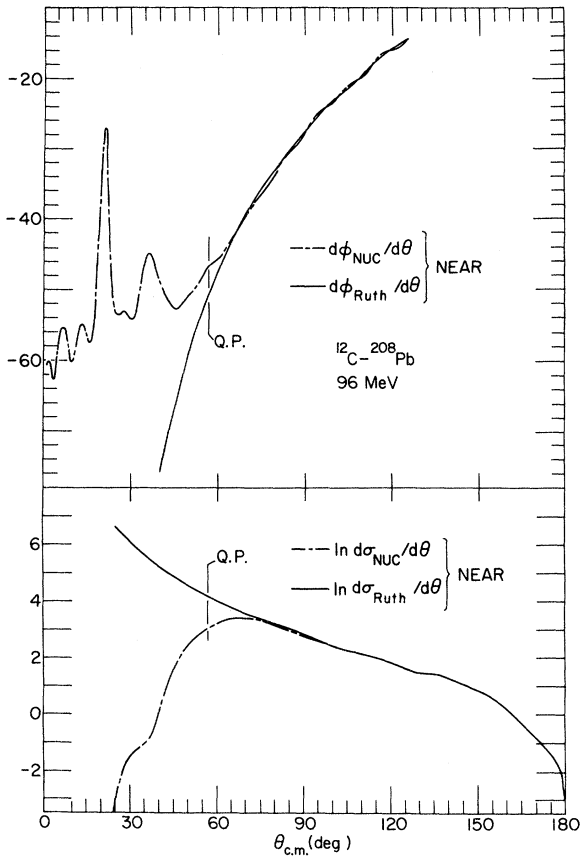

FIG. 11. The upper plot shows derivatives of phases of the near-nuclear amplitude $f_N(\theta) - f_{R,N}(\theta)$ (dash-dot) and near-Rutherford amplitude (solid) for 96 MeV ^{12}C on ^{208}Pb. The lower plot shows logarithmic plots of the near-nuclear (dot-dash) and near-Rutherford (solid) angular distributions. Again the quarter-point angle is shown.

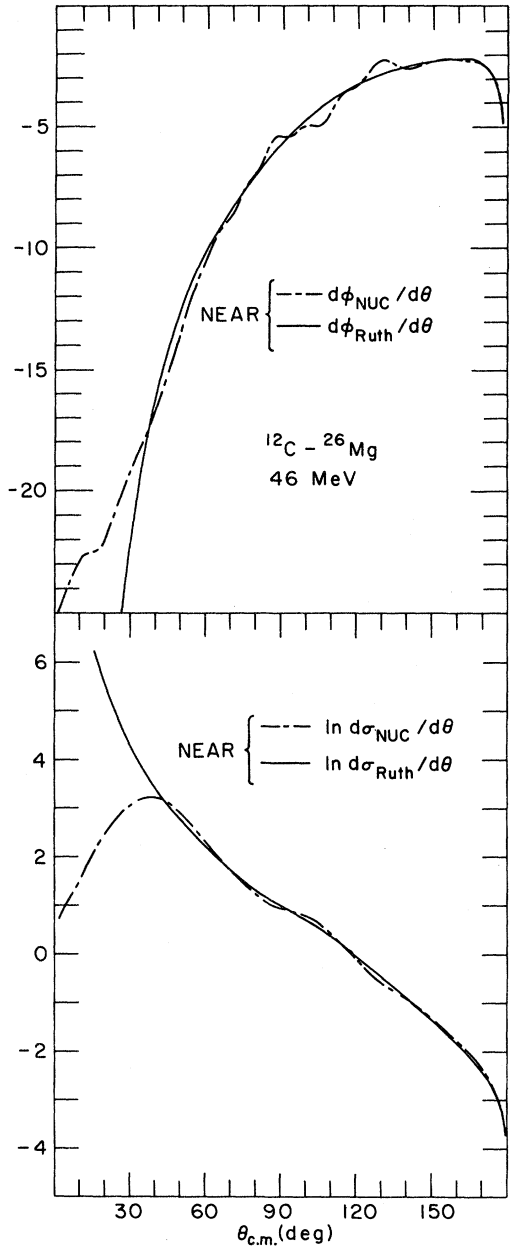

FIG. 12. The same plots appear here for 46 MeV ^{12}C on ^{26}Mg as appeared for ^{96}MeV ^{12}C on ^{208}Pb in the previous figure (Fig. 11).

$\theta \gtrsim \tan^{-1}(\eta/L)$, Eq. (28) for the absorptive nuclear amplitude can therefore be expected to approximate $-f_{\mathrm{Ruth}}(\theta)$. This discussion is offered as a heuristic argument for the formation of a diffractive or Fresnel[2] shadow for $\theta \gtrsim \tan^{-1}(\eta/L)$ and is supported by calculations shown in Figs. 11 and 12. For the ^{12}C-^{208}Pb case previously discussed, Fig. 11 shows the near-nuclear angular distribution and the phase derivative of the near-nuclear amplitude

along with the same qualities for the Rutherford amplitude. Obviously, the near-nuclear and near-Rutherford amplitudes are approximately equal for angles somewhat greater than the quarter-point angle indicated. Figure 12 shows the same quantities for the 46 MeV ^{12}C-^{26}Mg case, and the same observation made for the ^{12}C-^{208}Pb calculation is valid. It is this near cancellation of the near-side Rutherford and nuclear amplitudes in the presence of strong absorption which generates the diffractive shadow.

Further insight follows from the identification of the derivative of the phases of the far and near amplitudes with the "local angular momentum". This is in analogy with the semiclassical identification of the derivative of the phase of a one-dimensional traveling wave with the local linear momentum. The validity of this identification for the Rutherford amplitude follows from Eqs. (29) and (30), but it is less immediate when there is same-side interference where both the magnitude and phase of a single-side amplitude may vary rapidly. This is apparent in the correlation of structure in the near-side phase derivatives in Figs. 8 and 10, with structure in the near-side angular distributions in Figs. 8 and 9. This structure is presumably ascribable to interference between the Coulomb and nuclear amplitudes in the shadow region where they pass back and forth through one another as indicated in Figs. 11 and 12. Again, the structure in the phase derivative of the near-nuclear amplitude in Fig. 11 is closely correlated with structure in the near-nuclear angular distribution, most of which is not shown. However, even in the presence of this interference oscillation the phase derivative can be qualitatively useful.

The short-range nuclear interaction requires that the nuclear amplitude, $(\tilde{S}_l - 1)/2ik$ in Eq. (24), decrease rapidly to zero as l increases beyond the angular momenta describing peripheral collisions. This limits the angular momentum content in the near-nuclear amplitude, which is reflected in their phase derivatives peeling away from the Rutherford phase derivatives which continue to larger negative values with decreasing scattering angle. For the ^{12}C-^{208}Pb calculation, shown in Fig. 11, $|d\phi_{\mathrm{NUC}}/d\theta| \approx 60$ at $\theta \approx 0$, and $l \approx 60$ is approximately the maximum angular momentum contained in the nuclear amplitude. This follows from the plot of the reflection coefficient in Fig. 8 which shows $|\tilde{S}_{60}| \approx 1$. For ^{12}C-^{26}Mg, $|d\phi_{\mathrm{NUC}}/d\theta| \approx 25$ at $\theta \approx 0$ and again $l = 25$ is in the upper shoulder of the reflection coefficient shown in Fig. 10. For our arguments concerning the qualitative behavior or $\sigma/\sigma_{\mathrm{Ruth}}$ it is important to note that the magnitude of the phase derivative of the near-nuclear amplitude always lies below that of near-Coulomb amplitude in the angular region where they differ appreciably. Again, this is presumably a reflection of the limited angular momentum content of the nuclear amplitude and simply means the phase of near-nuclear amplitude is changing less rapidly than that of the Coulomb amplitude.

One might guess that the deep shadow starts at the scattering angle where the local angular momentum of the near-nuclear amplitude lies in the lower shoulder of the reflection coefficient, i.e., for $S_l \approx 0$ where $l \lesssim L$ the shadow starts at the angle $\theta_S = 2\tan^{-1}(\eta/L)$. This would result from the arguments following Eq. (28) and is also consistent with the most naive physical argument which says absorbed partial waves generate the shadow.

By way of defining the "start" of the deep shadow we note that in both Figs. 11 and 12, the near-nuclear angular distribution approaches the Rutherford angular distribution with which it coalesces shortly after reaching its maximum. Therefore we associate this maximum with the start of the deep shadow. In Fig. 11, $d\sigma_{\mathrm{NUC}}/d\theta$ peaks at $\theta_S = 66°$ where $d\phi_{\mathrm{NUC}}/d\theta \approx -42$, and in Fig. 8 we see that $L \approx 42$ indeed falls in the lower shoulder of the reflection coefficient. For 96 MeV ^{12}C-^{208}Pb scattering $\eta = 27.4$ and $2\tan^{-1}(\eta/L) = 2\tan^{-1}(27.4/42) \approx 66° = \theta_S$, which might be called the "strong absorption angle". The same analysis may be repeated for the 46 MeV ^{12}C-^{26}Mg case in Fig. 12; $d\sigma_{\mathrm{NUC}}/d\theta$ peaks at $\theta_S = 38°$ where $d\phi_{\mathrm{NUC}}/d\theta \approx 17 = L$ which again falls in the lower shoulder of the reflection coefficient shown in Fig. 10. Further, $2\tan^{-1}(\eta/L) = 2\tan^{-1}(5.79/17) \approx 38° = \theta_S$, the strong absorption angle.

We now have the following qualitative picture of near-side elastic scattering. There is a diffractive shadow extending forward to the strong absorption angle where the near-nuclear amplitude peaks and one begins to probe angular momenta in the refractive region of the reflection coefficient. Within the angle θ_S the near-nuclear angular distribution fall rapidly and the total angular distribution rapidly climbs to approximate the Rutherford cross section which is dominant at forward angles. As will be discussed shortly, the forward angle structure in $\sigma/\sigma_{\mathrm{Ruth}}$ can be understood in terms of the limited angular momentum content of the nuclear amplitude.

The near cross section in the shadow is small and arises from reflection at, or within, the interaction surface. Unlike a Coulomb-rainbow–near-side angular distribution which is determined by peripheral S-matrix elements, the (local) angular momentum in the absorptive shadow decreases with increasing scattering angle. As mentioned earlier, the resulting lower centripetal barrier can allow the reflected components to emanate

from the interior of the interaction region. Therefore, back-angle near-side scattering can probe the interior of the interaction region. This qualitative picture of near-side scattering follows from the absorptive nature of heavy-ion elastic scattering and does not depend on the detailed nature of the interaction of two appreciably overlapping ions, which is presumably complicated by effects such as those arising from the Pauli exclusion principle. On the other hand, quantitative features of large-angle near-side dominated scattering can be expected to depend sensitively on details of the interaction.

Forward of the strong absorption angle the angular distribution is best discussed in the customary fashion as the ratio of the near cross section to Rutherford, i.e., we consider

$$g(\theta)=\frac{f_N(\theta)}{f_{R,N}(\theta)}=1+\frac{\tilde{f}_N(\theta)}{f_{R,N}(\theta)}$$
$$=1+\tilde{g}(\theta)\,, \tag{32}$$

where $\sigma_{\text{near}}/\sigma_{\text{Ruth,near}}=|g(\theta)|^2$. For a near-side dominated cross section this is virtually identical to $\sigma/\sigma_{\text{Ruth}}$. Since $|\tilde{f}_N(\theta)|$ peaks at $\theta\approx\theta_S$, where $\tilde{f}_N(\theta)\approx -f_{R,N}(\theta)$, while $|f_{R,N}(\theta)|$ continues to increase with decreasing angles, $|\tilde{g}(\theta)|<1$ for $\theta<\theta_S$. We now write

$$\tilde{g}(\theta)=|\tilde{g}(\theta)|\,e^{i\Phi(\theta)}\,, \tag{33}$$

where

$$\Phi(\theta)=\tilde{\phi}_N(\theta)-\phi_{R,N}(\theta) \tag{34}$$

is the difference of the phases of the near-nuclear and Rutherford amplitudes. From both Figs. 11 and 12 it is obvious that $d\Phi/d\theta>0$ for $\theta<\theta_S$, which implies $\Phi(\theta)$ decreases as θ decreases from θ_S. This, in turn, implies that $\tilde{g}(\theta)$, considered as a complex phasor, rotates in the clockwise direction as θ decreases from θ_S starting with the phase π.

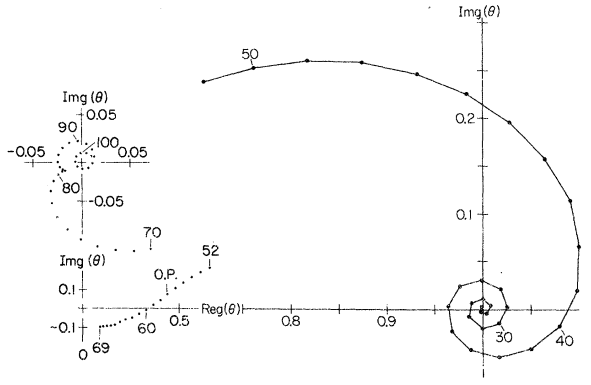

FIG. 13. Argand plot of $f_N(\theta)/f_{R,N}(\theta)=g(\theta)$ for 96 MeV ^{12}C on ^{208}Pb. The running variable is the scattering angle θ with $g(\theta)$ shown at degree steps.

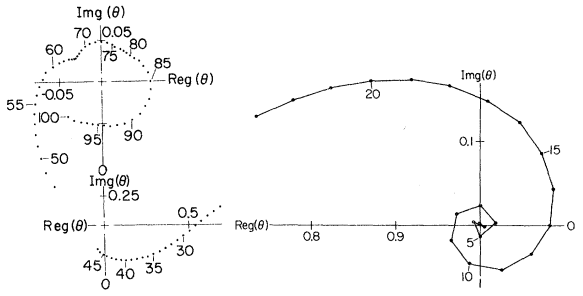

FIG. 14. For 46 MeV ^{12}C on ^{26}Mg this figure contains the same plots as Fig. 13 shows for 96 MeV ^{12}C on ^{208}Pb.

Since $\tilde{f}_N(\theta)$ and $f_{R,N}(\theta)$ generally diverge both in magnitude and phase, $\tilde{g}(\theta)$ rotates at an ever increasing rate as it shrinks in magnitude. It is this behavior of $\tilde{g}(\theta)$ which leads to the Cornu-spiral-like appearance of the complex behavior of $g(\theta)$ shown in Figs. 13 and 14 and this, in turn, is responsible for $\sigma/\sigma_{\text{Ruth}}$ oscillating with increasing magnitude and period, as θ increases, until it falls from its last local maximum as the phase of $\tilde{g}(\theta)$ increases from 0 to approximately π at the strong absorption angle θ_S.

This completes our discussion of the near-side amplitude. The qualitative picture which has emerged is just Frahn's Fresnel diffraction interpretation of $\sigma/\sigma_{\text{Ruth}}$. It should be remembered, however, that the angular distribution for an angle $\theta<\theta_S$ (the strong absorption angle), the nuclear amplitude is determined by the refractive S-matrix elements, i.e., the peripheral nonzero S-matrix elements. This means the quantitative behavior of $\sigma/\sigma_{\text{Ruth}}$ in the forward direction depends on the detailed behavior of the peripheral S matrix. However, the qualitative behavior of $\sigma/\sigma_{\text{Ruth}}$ for a near-side dominated angular distribution is determined by absorption, and not by the diffractive aspects of the S matrix such as the Coulomb rainbow.

We do not contend that the angular distributions discussed in this paper exhaust all the possibilities; however, it is hoped that the concepts used in their discussion are sufficiently broad to be generally useful.

ACKNOWLEDGMENTS

Discussions with K. McVoy and P. Moffa were useful in clarifying both the physics and the presentation of this paper. I am grateful to H. Wolter for sharing his most impressive Regge-pole search code and for patient advice concerning its operation. F. Paige provided appreciated suggestions for the evaluation of the integral arising in the isolation of positive and negative-deflection-angle contributions to the Rutherford amplitude. I thank the Oak Ridge and Saclay groups for sending me copies of their work prior to publication.

*Work supported by the Energy Research and Development Administration.

[1]J. S. Blair, Phys. Rev. 95, 1218 (1954).
[2]W. E. Frahn, Phys. Rev. Lett. 26, 568 (1971); Ann. Phys. (N.Y.) 72, 524 (1972).
[3]R. A. Broglia, S. Landowne, and A. Winther, Phys. Lett. B 40B, 293 (1972); D. A. Goldberg and S. M. Smith, Phys. Rev. Lett. 29, 500 (1972).
[4]D. A. Goldberg and S. M. Smith, Phys. Rev. Lett. 33, 715 (1974).
[5]R. da Silveira, Phys. Lett. B 45B, 211 (1973).
[6]N. Rowley and C. Marty, Phys. Lett. B 55B, 430 (1975).
[7]J. A. McIntyre, K. H. Wang, and L. C. Becker, Phys. Rev. 117, 1337 ((1960).
[8]R. C. Fuller and K. W. McVoy, Phys. Lett. B 55B, 121 (1975).
[9]R. C. Fuller, Phys. Lett. B 57B, 217 (1975).
[10]W. A. Friedman, K. W. McVoy, and G. W. T. Shuy, Phys. Rev. Lett. 33, 308 (1974).
[11]Notation for the functions used in this paper follow Refs. 12 or 13.
[12]*Handbook of Mathematical Functions*, edited by M. Abramowitz and I. Stegun (National Bureau of Standards, Washington, D. C., 1964).
[13]*Higher Transcendental Functions* (Bateman Manuscript Project), edited by A. Erdélyi (McGraw-Hill, New York, 1953), Vol. 1.
[14]R. P. Boas, Jr., and R. C. Buck, *Polynomial Expansions of Analytic Functions* (Academic, New York, 1964).
[15]I thank E. Auerbach for helping me use his optical model code ABACUS.
[16]M. C. Mermaz, Saclay report, 1973 (unpublished); see also M.-C. Lemaire, M. C. Mermaz, H. Sztark, and A. Cunsolo, Phys. Rev. C 10, 1103 (1974).
[17]T. Tamura and H. H. Wolter, Phys. Rev. C 6, 1976 (1972).
[18]K. W. McVoy, Phys. Rev. C 3, 1104 (1971).
[19]R. C. Fuller, Nucl. Phys. A A216, 199 (1973).
[20]J. V. Maher *et al.*, in *Proceedings of the Fifth International Conference on Nuclear Reactions Induced by Heavy Ions, Heidelberg, 1969*, edited by R. Bock and W. R. Hering (North-Holland, Amsterdam, 1970), p. 60.
[21]N. Austern, Ann. Phys. (N.Y.) 15, 299 (1961).
[22]R. C. Fuller and Y. Avishai, Nucl. Phys. A A222, 365 (1974).
[23]K. W. Ford and J. A. Wheeler, Ann. Phys. (N.Y.) 7, 259 (1959).
[24]M. Conjeaud, S. Harar, E. F. da Silveira, and C. Volant, Saclay report, 1975 (unpublished).
[25]J. B. Ball *et al.*, Oak Ridge report, 1975 (unpublished).
[26]K. W. McVoy, in *Classical and Quantum Mechanical Aspects of Heavy Ion Collisions*, edited by H. L. Harney, P. Braun-Munzinger, and C. K. Gelbke (Springer, Heidelberg, 1975), p. 127.